

Local Hemodynamic Forces After Stenting: Implications on Restenosis and Thrombosis

Jaryl Ng¹; Christos V. Bourantas^{2,3}; Ryo Torii⁴; Ang Hui Ying¹; Erhan Tenekecioglu⁵; Patrick W. Serruys^{5,6}; Nicolas Foin^{1,7*}

Affiliations:

1. National Heart Centre Singapore, Singapore
2. Department of Cardiovascular Sciences, University College London, London, United Kingdom
3. Department of Cardiology, Barts Health NHS Trust, London, United Kingdom
4. Department of Mechanical Engineering, University College London, London, United Kingdom
5. Thoraxcenter, Erasmus MC, Rotterdam Erasmus University, Netherlands
6. National Heart & Lung Institute, Imperial College London, United Kingdom
7. Duke-NUS Medical School, National University of Singapore, Singapore

* Corresponding author

Adj. A/Prof. Nicolas Foin, PhD

National Heart Research Institute Singapore

5 Hospital Drive, Singapore 169609

Email: Nicolas.foin@gmail.com

Highlights

- Stent restenosis and thrombosis are major complications that can develop after percutaneous coronary intervention and are associated with risks of reintervention and potential acute coronary events.
- Hemodynamic forces trigger biological pathways that are involved in both stent thrombosis and restenosis.
- Effort should be made to design drug-eluting stents and bioresorbable scaffolds that will have an optimal hemodynamic profile so as to improve their safety and reduce the incidence of stent/scaffold related adverse events.
- Optimal stent/scaffold expansion is associated with improved local hemodynamics and low incidence of adverse events.

Abstract

Local hemodynamic forces are well-known to modulate atherosclerotic evolution, which remains one of the largest cause of death worldwide. Percutaneous coronary interventions with stent implantation restores blood flow to the downstream myocardium and is only limited by stent failure caused by restenosis, stent thrombosis, or neoatherosclerosis. Cumulative evidence has shown that local hemodynamic forces affect restenosis and the platelet activation process, modulating the pathophysiological mechanisms that lead to stent failure. This article first covers the pathophysiological mechanisms through which wall shear stress regulates arterial disease formation/neointima proliferation and the role of shear rate on stent thrombosis. Subsequently, the article reviews the current evidence on (1) the implications of stent design on the local hemodynamic forces, and (2) how stent/scaffold expansion can influence local flow, thereby affecting the risk of adverse events.

Key Words: hemodynamics, percutaneous coronary intervention, stents, thrombosis

List of Abbreviations

PCI Percutaneous Coronary Intervention
3D Three-Dimensional
OCT Optical Coherence Tomography
IVUS Intravascular Ultrasound
ESS Endothelial Shear Stress
CFD Computational Fluid Dynamics
BMS Bare Metal Stent
DES Drug Eluting Stent
BVS Bioresorbable Vascular Scaffold
vWF Von Willebrand Factor
BRS Bioresorbable Scaffold
MLD Minimum Lumen Diameter
DoCE Device Orientated Composite Endpoint
ISA Incomplete Strut Apposition

Introduction

Advances in stent technology, drug polymer biocompatibility, and design have improved the safety and efficacy of coronary stent devices. Despite these advances, restenosis and device thrombosis remain a major concern and are still affecting longterm clinical outcomes.¹ Randomized trials and clinical registries show that the rate of stent thrombosis is <1% after 1 year, and the restenosis rates remain at ≈5%.² Nevertheless, the cumulative incidences of these events in the long term still remain substantial. Hence, it is crucial to identify the causes of stent/scaffold failure and understand how the hemodynamic environment impacts clinical outcomes postpercutaneous coronary intervention (PCI). With current high-resolution intravascular imaging, geometrically accurate representation of patient-specific coronary anatomy can be reconstructed for blood flow simulation, enabling precise endothelial shear stress (ESS) maps to be generated (Figure 1). Patient-specific biomechanical forces can then be quantified to investigate the pathophysiological implications of the flow patterns in stented/scaffolded segments and their role in neointimal hyperplasia and device thrombosis.⁴ This article will first define the metrics of local hemodynamics and introduce the main pathophysiological mechanisms, followed by a summary on the evidence about the role of the local hemodynamics on stent thrombosis and restenosis.

Metrics of Local Hemodynamics

Shear Rate

Shear rate is defined as the local velocity gradient between adjacent blood flow streamlines (Figure 2) and provides a quantitative representation of local flow disturbance. Shear rate is also one of the main regulators of platelet activation and thrombosis.^{6,7} In medium- to large-sized arteries, physiological shear rate falls within the range of 100 to 1000 s⁻¹.⁸ In silico and in vivo studies have shown that in stented/scaffolded segments, the rigid protruding and malapposed struts create flow obstructions that disrupt blood flow, resulting in flow separation and shear rates >2000 s⁻¹.⁹⁻¹²

Endothelial Shear Stress

ESS is estimated by multiplying the shear rate at the wall surface with the viscosity of blood (Figure 2) and represents the tangential frictional stress on the vessel wall imposed by the flowing blood. In vivo evaluations of ESS using computational fluid dynamic methods have shown that its distribution predicts atherosclerotic lesion development.¹³⁻¹⁷ Low and oscillatory ESS is a known modulator of arterial wall physiology, specifically via impaired endothelial cell function where low ESS has been shown to regulate gene expression and vascular proinflammatory response through multiple mechanotransduction pathways.^{18,19}

Hemodynamics Impact on Disease Process

Low ESS and Arterial Disease Development

The endothelium senses changes in ESS via several mechanotransduction processes that involve activation/release of signalling proteins in endothelial cells and smooth muscle cells, which in turn regulate vessel wall physiology.²⁰⁻²⁵ The type and magnitude of response are determined by the magnitude and direction of ESS.²⁶ Experimental studies have demonstrated that low ESS (<10 dynes/cm²) causes misalignment of the endothelium^{27,28} and disruption of cell-cell junctions.²⁹⁻³¹ This increases the permeability of the endothelium to circulating lipids and inflammatory regulators.³²⁻³⁴ In addition, low ESS decreases vasodilator,²⁵ fibrinolytics,³⁵ and antioxidants³⁶ and increases expression of cell adhesion molecules,²² growth factors,³⁷

vasoconstrictors,³⁸ oxidative species,³⁹ proteolytic enzymes,⁴⁰ and acute inflammatory mediators.⁴¹ This leads to endothelial dysfunction, vessel inflammation, and smooth muscle cells proliferation, contributing to plaque growth and arterial expansive remodeling.¹⁴ The behavior of smooth muscle cells is regulated by the interaction with endothelial cells but also by mechanical forces, such as shear stress. ESS leads to the release of platelet-driven growth factor and transforming growth factor which causes smooth muscle cell proliferation and migration, subsequently resulting in neointimal hyperplasia and restenosis.^{14,26,38} When there is no endothelium, Liu and Goldman⁴² demonstrated that smooth muscle cell migration is significantly suppressed under laminar flow conditions compared with regions that are exposed to recirculating and unsteady flow.

Shear modification has been shown to modulate plaque progression and the degree of inflammation in animal models.^{18,43} Low and oscillating ESS has been reported to accelerate vulnerable atherosclerotic plaque formation.^{18,19} In a recent experimental study using intracoronary shear-modifying stents in hypercholesterolemic pigs, Pedrigo et al⁴⁴ reported an ~3- fold increase in plaque burden distal to the shear-modifying stents compared with both proximal segment and the control arteries. Advanced coronary plaques were collocated mostly downstream of the shear-modifying stents, in regions of low ESS.⁴⁴ Although low ESS alone has been shown to increase plaque progression, a combination of low and oscillatory ESS is considered to be particularly atherogenic. Flow simulations on intravascular ultrasound–derived vessels of patients with coronary artery disease demonstrated that low and oscillatory ESS can cause plaques to evolve into a more vulnerable phenotype compared with low ESS only because of more inflammation and necrotic core progression.⁴⁵

The Table summarizes studies that have examined the impact of low ESS on atherosclerosis and restenosis. Most studies associated regions of low ESS with increased plaque burden or atherosclerosis plaque progression.

Low ESS and Restenosis Post-PCI

Studies have reported that there is also an inverse correlation between baseline ESS and neointimal thickness at follow-up (ie, low ESS increases neointimal proliferation). In the study conducted by Wentzel et al,⁵⁰ blood flow simulation was performed in segments implanted with bare metal stents (BMS). The ESS distribution was estimated on the reconstructed surfaces of stented vessel segments after implantation and at 6-month follow-up. An inverse association was found between baseline ESS and neointima formation at 6-month follow-up.⁵⁰ These findings were confirmed in several other studies.^{3,50,52,53,58,59} Papafaklis et al⁵³ investigated the implications of the local hemodynamic forces on neointimal response in BMS and first-generation drug-eluting stents (DES). The study reported an inverse correlation between ESS and neointima response in BMS while in DES vessels, wall response was shown to depend on the antiproliferative drug. Sirolimus seems to reduce the amount of positive cell cycle regulators and increase the amount of cell cycle inhibitors, leading to inhibited cell migration, proliferation, and desensitization of the cells to the effects of low ESS.

The PREDICTION study (Prediction of Progression of Coronary Artery Disease and Clinical Outcome Using Vascular Profiling of Shear Stress and Wall Morphology) was the largest ESS study investigating the implications of the local hemodynamic forces on the healing response after BMS and first-generation DES in vivo. The relationship between postprocedural ESS and neointimal in-stent hyperplasia was investigated by comparing the 3-dimensional reconstructed stented segments of 374 patients at baseline immediately after stent implantation and 6- to 10-month follow-up.^{17,57} The study demonstrated an inverse relationship between ESS and neointima response in BMS while in DES, the neointima tissue was too limited for assessment of the association between ESS and neointima tissue.⁵⁷ Bourantas et al⁵⁶ have also investigated the association between ESS and neointima proliferation using serial intravascular ultrasound imaging in 43 patients

implanted with either BMS or biolimus-eluting stents at baseline and 13-month follow-up. Negative correlations were noted between ESS and neointima thickness in both groups. There was also a negative correlation between ESS and the percentage of neointimal necrotic core component ($P=0.015$) in BMS while the limited neointima formation impeded the evaluation of the effect of ESS on neointima characteristics in DES.

Optical coherence tomography–based reconstruction was used to assess the implications of the ESS on neointima response in 12 patients implanted with an everolimus-eluting bioresorbable vascular scaffold (BVS; Absorb BVS; Abbott Vascular, Santa Clara, CA). In this analysis, the optical coherence tomography data acquired at baseline and 1-year follow-up were used to model vessel geometry.⁵⁵ The authors showed that the protruding struts resulted in low ESS in the areas between the struts and high ESS at the top of the struts. A strong negative correlation was observed between baseline ESS and neointimal thickness at follow-up; and increased neointima proliferation was found in the areas between the struts where the ESS was. This resulted in a smoothing of the rugged luminal surface and a homogenization of the ESS at 2-year follow-up.⁵⁵

Recently, Torii et al⁶⁰ evaluated the implications of the local flow patterns on neoatherosclerotic lesion formation in 35 patients implanted with either BMS or DES. The patients were admitted with coronary events attributed to stent failure and had neoatherosclerotic lesions based on optical coherence tomography images. An inverse association was noted between ESS and the incidence and burden of lipid-rich neoatherosclerotic tissue ($P<0.001$). Segments exposed to low ESS (<1 Pa) were more likely to exhibit macrophage accumulations, thrombus, or neointima discontinuities compared with those exposed to normal or high ESS ($P<0.001$). These results indicate that local ESS also plays a role in the regulation of neoatherosclerosis lesion formation in stented segments⁶⁰ (Figure 3).

Shear Rate Modulation of Platelet Activation and Thrombosis

Shear rate seems to play an important role on vessel physiology and determines the concentration of platelets and adhesion proteins near the vessel wall. In segments exposed to high shear rate, red blood cells cause platelets displacement toward the vessel wall via a process called margination. The accumulation of platelets and adhesion proteins near the vessel wall creates a prothrombotic environment.^{61–63}

When adhesion proteins like Von Willebrand factor and fibrinogen come in contact with a thrombogenic surface (ie, ruptured plaques and stent struts), a clot cascade is triggered. Once the adhesion proteins attach to the thrombogenic surface, they stimulate activated platelets to bind to the surface. At high shear rates, the globular structure of the Von Willebrand factor elongates into a string structure,^{64–67} increasing the amount of platelet binding sites on the molecule. With high shear rates ($\approx 10\,000\text{ s}^{-1}$), Von Willebrand factor strings combine to form nets that further increase the amount of platelet binding sites by $\approx 10\,000\times$.^{66,68} The attracted platelets are exposed to high ESS, which shortens their activation time.⁶⁹ As the thrombus grows, more Von Willebrand factor nets are formed which subsequently increase the number of bound platelets. This positive feedback loop results in thrombus formation.⁶⁹

Stent-Induced Hemodynamic Changes During PCI

In the BMS era, excessive neointimal proliferation was a major drawback that caused early restenosis.⁷⁰ With the introduction of DES, the occurrence of restenosis has been significantly reduced. However, in-stent thrombosis has remained an issue observed at both short- and long-term follow-up. It was reported that strut dimensions and the distance of the struts from the vessel wall affect stent thrombogenicity more than the presence of drug coatings.¹¹ Although stent thrombosis may have a relatively low incidence (0.6%–3.4%),⁷¹ it is still the most feared complication after PCI because of the associated mortality risk for the patients.⁷² Studies have revealed that the major causes of early stent thrombosis (<30 days) are largely because of stent underexpansion and malapposition while late stent thrombosis (>30 days) is found frequently with late remodeling, stent strut malapposition, and delayed endothelial coverage.⁷¹

Stent Design

Stent design has an impact on the flow dynamics in stented segments. Strut thickness, in particular, is a major factor affecting local shear rate and ESS post-PCI. Large strut thickness increases the amount of foreign material in the lumen and leads to flow disturbances, flow separation, and areas of recirculation zones, thereby increasing the risk of stent thrombosis.^{9–12,55,73} Models have shown that the maximal distance between the helical rings should be at least 6× the strut thickness to recover any laminar flow in the interstrut zones.⁷⁴ Smaller strut thickness can improve re-endothelialization and reduce peristrut inflammation and fibrin deposition.^{75–77} In the BMS era, clinical studies have reported improved outcomes in patients implanted with thin strut stents.^{78–81} Flow separation distance was also found to be longer in nonstreamlined struts (rectangular) compared with streamlined struts (circular/ovoid).⁸² Polymer coating is another essential part of stent design that can affect stent's thrombogenicity. Otsuka et al⁸³ observed in an ex vivo model that the fluoropolymer-coated Xience DES showed a significantly lower percentage of a thrombus-occupied areas compared with a DES with contemporary biodegradable coatings. Kolandaivelu et al¹¹ investigated the implications of stent design and drug coating on the incidence of stent thrombosis by deploying DES and BMS with identical design but different strut thickness in ex vivo perfusion models. Results indicated that DES with a biocompatible drug coating had a 0.65-fold lower thrombogenicity compared with BMS while thicker struts stents were 1.5× more thrombogenic than thin strut stents with the same design.¹¹

Current bioresorbable scaffolds (BRS) have thicker struts ($\geq 150 \mu\text{m}$) compared with second-generation metallic DES ($\leq 100 \mu\text{m}$). One of the most widely examined BRS is the Abbott Vascular's Absorb BVS, which is fabricated from a poly-L-lactic acid backbone. The Absorb BVS has a strut thickness of $156 \mu\text{m}$ and a width of $190 \mu\text{m}$ while the Xience DES has a total strut thickness of $89 \mu\text{m}$. Because of the lower elastic modulus and tensile strength of the bioresorbable materials, thicker struts are often required in BRS to achieve a radial force similar to that of conventional metallic platforms.^{84–86}

Studies have shown more extensive neointimal hyperplasia and late lumen loss in BRS compared with DES at showed >50% increase in maximum shear rate values with protruding stent struts¹⁰ compared with embedded struts. These flow patterns around indented struts are commonly associated with increased platelet adhesion^{11,93} and inflammatory response,⁹⁴ as well as reduced re-endothelialization.^{75,95–97} short-term follow-up.^{85,87–91} Large strut size and other factors, such as scaffold underexpansion, incomplete scaffolding, and the acidic environment during polymer dissolution, may play a role in causing late lumen loss in BRS device. It has been hypothesized that the large strut profile of current generation of BRS is harder to embed in the tissue, hence creating a larger obstacle for blood flow.⁹² Computational flow simulations showed >50% increase in maximum shear rate values with protruding stent struts¹⁰ compared with embedded struts. These flow patterns around indented struts are commonly associated with increased platelet adhesion^{11,93} and inflammatory response,⁹⁴ as well as reduced re-endothelialization.^{75,95–97}

Under Expansion

Stent underexpansion is usually quantified by the postprocedural diameter stenosis in quantitative coronary angiography and intravascular imaging. This is done by measuring the minimum lumen area of the stent/scaffold segment and relative percentage area stenosis. Underexpansion can be caused by inappropriate lesion preparation and postdilatation of the implanted stent/scaffold with too small balloons or insufficient pressure, particularly in fibrotic or fibrocalcific lesion types.⁹⁸ Stent underexpansion leads to shear stress concentration on the edges of the stent struts and higher jet and shear rate in the underexpanded segment, which may increase the risk of stent thrombosis.⁹⁹ Stent underexpansion has been commonly associated with early stent thrombosis (>30 days).^{100–102} Fujii et al¹⁰¹ conducted an analysis on 15 patients admitted for stent thrombosis and compared them with 45 matched control patients with no stent thrombosis. The study showed that the stent cross-sectional area was significantly smaller in the stent thrombosis group than in the matched control patients (4.3 ± 1.6 versus 6.2 ± 1.9 mm²).¹⁰¹

Another study sought to compare the acute gain and late lumen loss between Absorb BVS and DES at 2-year follow-up. Thirty-three patients implanted with BVS and 26 patients implanted with the DES from the ABSORB B (ABSORB Clinical Investigation, Cohort B) and SPIRIT II (A Clinical Evaluation of the XIENCE V® Everolimus Eluting Coronary Stent System) trials were examined. Analysis showed similar acute gain (BVS: 1.23 ± 0.38 mm versus DES: 1.32 ± 0.26 mm; $P=0.29$) and similar in device late lumen loss at 2-year follow-up (BVS: 0.26 ± 0.19 mm versus DES: 0.22 ± 0.22 mm; $P=0.29$). However, patients implanted with BVS showed significantly lower in stent minimum lumen diameter compared with patients implanted with DES (BVS: 2.02 ± 0.26 mm versus DES: 2.22 ± 0.34 mm; $P=0.01$).¹⁰³ Suwannasom et al¹⁰⁴ investigated the postprocedural asymmetry, expansion, and eccentricity indices between DES and BVS and their impact on clinical outcomes at 1-year follow-up. Pre- and postprocedural intravascular ultrasound images from 470 patients were used to calculate the asymmetry index per lesion and eccentricity index per cross-section. DES was more symmetrical and concentric compared with the BVS group post procedure, with only 8% of BVS compared with 20% of DES achieving optimal scaffold/stent expansion ($P<0.001$). Although there was no difference in device-oriented composite end point at 1-year follow-up (BVS=5.2% versus DES=3.1%; $P=0.29$), postprocedural device asymmetry was associated with increased event rates, with analysis showing that asymmetry index >0.30 was an independent predictor of device-oriented composite end point (hazard ratio: 3.43; $P=0.037$).

In a recent study, Foin et al¹⁰⁵ compared the acute expansion behavior of DES and Absorb BVS in an in vitro artery lesion model. Results showed that stent eccentricity at the minimum lumen area was lower in the BVS compared with Xience metallic stent when deployed at nominal pressure (BVS: 0.71 ± 0.02 versus Xience: 0.81 ± 0.02 ; $P=0.004$). These anatomic differences were associated with increased shear rate and increased recirculation zones at the downstream of the underexpanded segment.¹⁰⁵ Computational fluid dynamic models have also demonstrated that even at the same diameter stenosis, an eccentric lesion induces larger recirculation. Therefore, when the stent is not symmetrically expanded, intravascular imaging should be considered to assess the final result.¹⁰⁶

Scaffold underexpansion has been shown to be also a predictor of events in the Absorb BVS. Puricel et al⁸⁴ investigated the incidence, clinical and angiographic features, as well as the possible mechanisms of stent thrombosis in 1305 patients implanted with BVS. The study revealed that a low postprocedural minimum lumen diameter and low reference diameters were predictors of stent thrombosis.⁸⁴ The risk of stent thrombosis increased rapidly for minimum lumen diameter <2.4 mm for the 2.5- to 3.0-mm BVS and <2.8 mm for BVS that had a 3.5-mm diameter.⁸⁴ However, when aggressive lesion preparation and aggressive device postdilatation was implemented, scaffold thrombosis at 1-year follow-up fell from 3.3% to 1.0% ($P=0.012$),⁸⁴ suggesting that the implantation technique could be the key to reducing scaffold thrombosis in BVS.

Malapposition

Malapposition, also known as incomplete stent apposition (ISA), can affect local flow and shear profile in the stented vessel. A stent strut is considered malapposed when is not in contact with the vessel wall. Malapposed stent struts disrupt the laminar flow and can generate regions of high shear rate (Figures 4 and 5)^{10,11,13} which are known to affect the risk of stent thrombosis.^{11,77,107} In an in vitro experiment, Kolandaivelu et al¹¹ showed that malapposed BMS showed a 1.5-fold increase in thrombogenicity compared with wellapposed stents (P=0.001).

Malapposition also reduces stent strut coverage. A recent study analyzed the impact of baseline strut-vessel wall ISA distance on strut coverage at follow-up. As ISA increases from <100 μm to 100 to 300 μm and finally to >300 μm , the percentage of uncovered struts at follow-up increased from 0% to 6.1% and 15.7%, respectively.¹⁰

Recently, reports have pointed to ISA as a possible mechanism leading to scaffold thrombosis in BRS.^{109–112} In one study, Gomez-Lara et al showed that malapposed BRS struts are more frequently uncovered compared with apposed struts (29% of ISA struts versus 1% of apposed struts) and that intraluminal masses (possible thrombus) were seen in malapposed BRS struts more often as compared with apposed struts (39% of ISA struts versus 2% apposed struts).^{93,113–115} Computational fluid dynamic analysis on stented/scaffolded segments demonstrated higher shear profiles in BRS compared with thin metallic DES, hence underlining the importance of imaging guidance, optimal expansion, and apposition during BRS implantation.⁹⁹

Conclusion

To summarize, suboptimal stent implantation affects the local hemodynamic forces and can lead to unfavorable clinical outcomes. Regions of low ESS after PCI are collocated with neointima and neoatherosclerosis formation. High shear gradients and flow disturbances have been shown to increase the risk of thrombosis. Therefore, effort should be made to optimize stent deployment and stent/scaffold designs to ensure an optimal hemodynamic profile and reduce the risk of complications after PCI.

Disclosures

N. Foin holds an appointment in Philips and is adjunct faculty in National Heart Research Institute Singapore/Duke-NUS. The other authors report no conflicts.

References

1. Stone GW, Ellis SG, Colombo A, Dawkins KD, Grube E, Cutlip DE, Friedman M, Baim DS, Koglin J. Offsetting impact of thrombosis and restenosis on the occurrence of death and myocardial infarction after paclitaxel-eluting and bare metal stent implantation. *Circulation*. 2007;115(22):2842-2847.
2. Byrne RA, Joner M, Kastrati A. Stent thrombosis and restenosis: what have we learned and where are we going? The Andreas Grüntzig Lecture ESC 2014. *European Heart Journal*. 2015;36(47):3320-3331.
3. Papafaklis MI, Bourantas CV, Farooq V, Diletti R, Muramatsu T, Zhang Y, Fotiadis DI, Onuma Y, Garcia Garcia HM, Michalis LK, Serruys PW. In vivo assessment of the three-dimensional haemodynamic micro-environment following drug-eluting bioresorbable vascular scaffold implantation in a human coronary artery: fusion of frequency domain optical coherence tomography and angiography. *EuroIntervention*. 2013;9:890. doi: 10.4244/EIJV9I7A147.
4. Thondapu V, Bourantas CV, Foin N, Jang I-K, Serruys PW, Barlis P. Biomechanical stress in coronary atherosclerosis: emerging insights from computational modelling. *European Heart Journal*. 2016.
5. Foin N, Torii R, Lee R, Mattesini A, Wong P, Di Mario C, Tenekecioglu E, Crake T, Bourantas C, Serruys PW. Simulation of flow and shear stress. In: Onuma Y, Serruys PW, eds. *Bioresorbable Scaffolds: From Basic Concept to Clinical Applications*. Boca Raton, FL: 2017:79–87.
6. Strony J, Beaudoin A, Brands D, Adelman B. Analysis of shear stress and hemodynamic factors in a model of coronary artery stenosis and thrombosis. *Am J Physiol*. 1993;265(5 Pt 2):H1787-H1796.
7. Badimon L, Badimon JJ, Turitto VT, Vallabhajosula S, Fuster V. Platelet thrombus formation on collagen type I. A model of deep vessel injury. Influence of blood rheology, von Willebrand factor, and blood coagulation. *Circulation*. 1988;78(6):1431-1442.
8. Hanson SR, Sakariassen KS. Blood flow and antithrombotic drug effects. *Am Heart J*. 1998;135(5 Pt 2 Su):S132-S145.
9. Duraiswamy N, Schoepfoerster RT, Moreno MR, Moore JE. Stented Artery Flow Patterns and Their Effects on the Artery Wall. *Annual Review of Fluid Mechanics*. 2006;39(1):357-382.
10. Foin N, Gutiérrez-Chico JL, Nakatani S, et al. Incomplete Stent Apposition Causes High Shear Flow Disturbances and Delay in Neointimal Coverage as a Function of Strut to Wall Detachment Distance: Implications for the Management of Incomplete Stent Apposition. *Circulation: Cardiovascular Interventions*. 2014;7(2):180-189.
11. Kolandaivelu K, Swaminathan R, Gibson WJ, Kolachalama VB, Nguyen-Ehrenreich KL, Giddings VL, Coleman L, Wong GK, Edelman ER. Stent thrombogenicity early in high-risk interventional settings is driven by stent design and deployment and protected by polymer-drug coatings. *Circulation*. 2011;123(13):1400-1409.
12. Foin N, Lee RD, Torii R, Gutiérrez-Chico JL, Mattesini A, Nijjer S, Sen S, Petraco R, Davies JE, Di Mario C, Joner M, Virmani R, Wong P. Impact of stent strut design in metallic stents and biodegradable scaffolds. *International Journal of Cardiology*. 2014;177(3):800-808.
13. Koskinas KC, Chatzizisis YS, Antoniadis AP, Giannoglou GD. Role of Endothelial Shear Stress in Stent Restenosis and Thrombosis: Pathophysiologic Mechanisms and Implications for Clinical Translation. *Journal of the American College of Cardiology*. 2012;59(15):1337-1349.
14. Chatzizisis YS, Coskun AU, Jonas M, Edelman ER, Feldman CL, Stone PH. Role of Endothelial Shear Stress in the Natural History of Coronary Atherosclerosis and Vascular Remodeling: Molecular, Cellular, and Vascular Behavior. *Journal of the American College of Cardiology*. 2007;49(25):2379-2393.
15. Stone PH, Coskun AU, Kinlay S, Clark ME, Sonka M, Wahle A, Ilegbusi OJ, Yeghiazarians Y, Popma JJ, Orav J, Kuntz RE, Feldman CL. Effect of endothelial shear stress on the progression of coronary artery disease,

- vascular remodeling, and in-stent restenosis in humans: in vivo 6-month follow-up study. *Circulation*. 2003;108(4):438-444.
16. Wentzel JJ, Gijzen FJH, Stergiopoulos N, Serruys PW, Slager CJ, Krams R. Shear stress, vascular remodeling and neointimal formation. *Journal of Biomechanics*. 2003;36(5):681-688.
 17. Stone PH, Saito S, Takahashi S, et al. Prediction of Progression of Coronary Artery Disease and Clinical Outcomes Using Vascular Profiling of Endothelial Shear Stress and Arterial Plaque Characteristics: The PREDICTION Study. *Circulation*. 2012;126(2):172-181.
 18. Cheng C, Tempel D, van Haperen R, van der Baan A, Grosveld F, Daemen MJAP, Krams R, de Crom R. Atherosclerotic Lesion Size and Vulnerability Are Determined by Patterns of Fluid Shear Stress. *Circulation*. 2006;113(23):2744-2753.
 19. Chatzizisis YS, Jonas M, Coskun AU, Beigel R, Stone BV, Maynard C, Gerrity RG, Daley W, Rogers C, Edelman ER, Feldman CL, Stone PH. Prediction of the localization of high-risk coronary atherosclerotic plaques on the basis of low endothelial shear stress: an intravascular ultrasound and histopathology natural history study. *Circulation*. 2008;117(8):993-1002.
 20. Cunningham KS, Gotlieb AI. The role of shear stress in the pathogenesis of atherosclerosis. *Laboratory investigation; a journal of technical methods and pathology*. 2005;85(1):9-23.
 21. Gimbrone MA, Topper JN, Nagel T, Anderson KR, Garcia-Cardena G. Endothelial dysfunction, hemodynamic forces, and atherogenesis. *Ann NY Acad Sci*. 2000;902:230-239.
 22. Zhou J, Wang KC, Wu W, Subramaniam S, Shyy JY, Chiu JY, Chiu JJ, Li JY, Chien S. MicroRNA-21 targets peroxisome proliferators-activated receptor- α in an autoregulatory loop to modulate flow-induced endothelial inflammation. *Proc Natl Acad Sci*. 2011;108:10355-10360.
 23. Garcia-Cardena G, Comander J, Anderson KR, Blackman BR, Gimbrone MA, Jr. Biomechanical activation of vascular endothelium as a determinant of its functional phenotype. *Proc Natl Acad Sci U S A*. 2001;98(8):4478-4485.
 24. Son DJ, Kumar S, Takabe W, Kim CW, Ni CW, Alberts-Grill N, Jang IH, Kim S, Kim W, Won Kang S, Baker AH, Woong Seo J, Ferrara KW, Jo H. The atypical mechanosensitive microRNA-712 derived from pre-ribosomal RNA induces endothelial inflammation and atherosclerosis. *Nat Commun*. 2013;4:3000.
 25. Wu W, Xiao H, Laguna-Fernandez A, Villarreal G, Jr., Wang KC, Geary GG, Zhang Y, Wang WC, Huang HD, Zhou J, Li YS, Chien S, Garcia-Cardena G, Shyy JY. Flow-Dependent Regulation of Kruppel-Like Factor 2 Is Mediated by MicroRNA-92a. *Circulation*. 2011;124(5):633-641.
 26. Van der Heiden K, Gijzen FJH, Narracott A, Hsiao S, Halliday I, Gunn J, Wentzel JJ, Evans PC. The effects of stenting on shear stress: relevance to endothelial injury and repair. *Cardiovascular Research*. 2013;99(2):269-275.
 27. Malek AM, Izumo S. Mechanism of endothelial cell shape change and cytoskeletal remodeling in response to fluid shear stress. *J Cell Science*. 1996;109:713-726.
 28. Melchior B, Frangos JA. Shear-induced endothelial cell-cell junction inclination. *Am J Physiol Cell Physiol*. 2010;299(3):C621-629.
 29. DePaola N, Davies PF, Pritchard WF, Florez L, Harbeck N, Polacek DC. Spatial and temporal regulation of gap junction connexin43 in vascular endothelial cells exposed to controlled disturbed flows in vitro. *Proc Natl Acad Sci*. 1999;96:3154-3159.
 30. Pfenniger A, Wong C, Sutter E, Cuhlmann S, Dunoyer-Geindre S, Mach F, Horrevoets AJ, Evans PC, Krams R, Kwak BR. Shear stress modulates the expression of the atheroprotective protein Cx37 in endothelial cells. *J Mol Cell Cardiol*. 2012;53(2):299-309.

31. Miao H, Hu YL, Shiu YT, Yuan S, Zhao Y, Kaunas R, Wang Y, Jin G, Usami S, Chien S. Effects of flow patterns on the localization and expression of VE-cadherin at vascular endothelial cell junctions: in vivo and in vitro investigations. *J Vasc Res.* 2005;42(1):77-89.
32. Staughton TJ, Lever MJ, Weinberg PD. Effect of altered flow on the pattern of permeability around rabbit aortic branches. *Am J Physiol Heart Circ Physiol.* 2001;281:H53-H59.
33. Cancel LM, Tarbell JM. The role of apoptosis in LDL transport through cultured endothelial cell monolayers. *Atherosclerosis.* 2010;208(2):335-341.
34. Kang H, Cancel LM, Tarbell JM. Effect of shear stress on water and LDL transport through cultured endothelial cell monolayers. *Atherosclerosis.* 2014;233(2):682-690.
35. Papadaki M, Ruef J, Nguyen KT, Li F, Patterson C, Eskin SG, McIntire LV, Runge MS. Differential Regulation of Protease Activated Receptor-1 and Tissue Plasminogen Activator Expression by Shear Stress in Vascular Smooth Muscle Cells. *Circ Res.* 1998;83:1027-1034.
36. Inoue N, Ramasamy S, Fukai T, Nerem RM, Harrison DG. Shear Stress Modulates Expression of Cu/Zn Superoxide Dismutase in Human Aortic Endothelial Cells. *Circulation Research.* 1996;79:32-37.
37. Conklin BS, Zhong DS, Zhao W, Lin PH, Chen C. Shear stress regulates occludin and VEGF expression in porcine arterial endothelial cells. *J Surg Res.* 2002;102:13-21.
38. Qiu Y, Tarbell JM. Interaction between Wall Shear Stress and Circumferential Strain Affects Endothelial Cell Biochemical Production. *J Vasc Res.* 2000;37:147-157.
39. Sorescu GP, Song H, Tressel SL, Hwang J, Dikalov S, Smith DA, Boyd NL, Platt MO, Lassegue B, Griendling KK, Jo H. Bone morphogenic protein 4 produced in endothelial cells by oscillatory shear stress induces monocyte adhesion by stimulating reactive oxygen species production from a nox1-based NADPH oxidase. *Circ Res.* 2004;95(8):773-779.
40. Gambillara V, Montorzi G, Haziza-Pigeon C, Stergiopoulos N, Silacci P. Arterial wall response to ex vivo exposure to oscillatory shear stress. *J Vasc Res.* 2005;42(6):535-544.
41. Fang Y, Shi C, Manduchi E, Civelek M, Davies PF. MicroRNA-10a regulation of proinflammatory phenotype in athero-susceptible endothelium in vivo and in vitro. *PNAS.* 2010;107:13450-13455.
42. Liu SQ, Goldman J. Role of blood shear stress in the regulation of vascular smooth muscle cell migration. *IEEE Transactions on Biomedical Engineering.* 2001;48(4):474-483.
43. Partridge J, Carlsen H, Enesa K, Chaudhury H, Zakkar M, Luong L, Kinderlerer A, Johns M, Blomhoff R, Mason JC, Haskard DO, Evans PC. Laminar shear stress acts as a switch to regulate divergent functions of NF- κ B in endothelial cells. *The FASEB Journal.* 2007;21(13):3553-3561.
44. Pedrigi RM, Poulsen CB, Mehta VV, et al. Inducing Persistent Flow Disturbances Accelerates Atherogenesis and Promotes Thin Cap Fibroatheroma Development in D374Y-PCSK9 Hypercholesterolemic Minipigs. *CLINICAL PERSPECTIVE*. *Circulation.* 2015;132(11):1003-1012.
45. Timmins LH, Molony DS, Eshtehardi P, McDaniel MC, Oshinski JN, Giddens DP, Samady H. Oscillatory wall shear stress is a dominant flow characteristic affecting lesion progression patterns and plaque vulnerability in patients with coronary artery disease. *Journal of The Royal Society Interface.* 2017;14(127).
46. Stone PH, Coskun AU, Kinlay S, Popma JJ, Sonka M, Wahle A, Yeghiazarians Y, Maynard C, Kuntz RE, Feldman CL. Regions of low endothelial shear stress are the sites where coronary plaque progresses and vascular remodelling occurs in humans: an in vivo serial study. *Eur Heart J.* 2007;28:705-710. doi: 10.1093/eurheartj/ehl575.
47. Samady H, Eshtehardi P, McDaniel MC, Suo J, Dhawan SS, Maynard C, Timmins LH, Quyyumi AA, Giddens DP. Coronary artery wall shear stress is associated with progression and transformation of atherosclerotic

- plaque and arterial remodeling in patients with coronary artery disease. *Circulation*. 2011;124(7):779-788.
48. Vergallo R, Papafaklis MI, Yonetsu T, et al. Endothelial shear stress and coronary plaque characteristics in humans: combined frequency-domain optical coherence tomography and computational fluid dynamics study. *Circ Cardiovasc Imaging*. 2014;7:905–911.
 49. Hung OY, Molony D, Corban MT, et al. Comprehensive assessment of coronary plaque progression with advanced intravascular imaging, physiological measures, and wall shear stress: a pilot double-blinded randomized controlled clinical trial of nebivolol versus atenolol in nonobstructive coronary artery disease. *J Am Heart Assoc*. 2016;5:e002764. doi: 10.1161/JAHA.115.002764.
 50. Wentzel JJ, Krams R, Schuurbiens JC, Oomen JA, Kloet J, van der Giessen WJ, Serruys PW, Slager CJ. Relationship between neointimal thickness and shear stress after Wallstent implantation in human coronary arteries. *Circulation*. 2001;103(13):1740-1745.
 51. Gijzen FJ, Oortman RM, Wentzel JJ, Schuurbiens JC, Tanabe K, Degertekin M, Ligthart JM, Thury A, de Feyter PJ, Serruys PW, Slager CJ. Usefulness of shear stress pattern in predicting neointima distribution in sirolimus-eluting stents in coronary arteries. *Am J Cardiol*. 2003;92:1325–1328.
 52. Papafaklis MI, Bourantas CV, Theodorakis PE, Katsouras CS, Fotiadis DI, Michalis LK. Relationship of shear stress with in-stent restenosis: Bare metal stenting and the effect of brachytherapy. *International Journal of Cardiology*. 2009;134(1):25-32.
 53. Papafaklis MI, Bourantas CV, Theodorakis PE, Katsouras CS, Naka KK, Fotiadis DI, Michalis LK. The Effect of Shear Stress on Neointimal Response Following Sirolimus- and Paclitaxel-Eluting Stent Implantation Compared With Bare-Metal Stents in Humans. *JACC: Cardiovascular Interventions*. 2010;3(11):1181-1189.
 54. Bourantas CV, Papafaklis MI, Lakkas L, et al. Fusion of optical coherence tomographic and angiographic data for more accurate evaluation of the endothelial shear stress patterns and neointimal distribution after bioresorbable scaffold implantation: comparison with intravascular ultrasound-derived reconstructions. *The International Journal of Cardiovascular Imaging*. 2014;30(3):485-494.
 55. Bourantas CV, Papafaklis MI, Kotsia A, et al. Effect of the Endothelial Shear Stress Patterns on Neointimal Proliferation Following Drug-Eluting Bioresorbable Vascular Scaffold Implantation: An Optical Coherence Tomography Study. *JACC: Cardiovascular Interventions*. 2014;7(3):315-324.
 56. Bourantas CV, Räber L, Zaugg S, et al. Impact of local endothelial shear stress on neointima and plaque following stent implantation in patients with ST-elevation myocardial infarction: A subgroup-analysis of the COMFORTABLE AMI-IBIS 4 trial. *International Journal of Cardiology*. 2015;186:178-185.
 57. Shishido K, Antoniadis AP, Takahashi S, Tsuda M, Mizuno S, Andreou I, Papafaklis MI, Coskun AU, O'Brien C, Feldman CL, Saito S, Edelman ER, Stone PH. Effects of Low Endothelial Shear Stress After Stent Implantation on Subsequent Neointimal Hyperplasia and Clinical Outcomes in Humans. *Journal of the American Heart Association*. 2016;5(9).
 58. Carlier SG. Augmentation of Wall Shear Stress Inhibits Neointimal Hyperplasia After Stent Implantation Inhibition Through Reduction of Inflammation? *Circulation*. 2003;107(21):2741.
 59. Richter Y. Dynamic flow alterations dictate leukocyte adhesion and response to endovascular interventions. *Journal of Clinical Investigation*. 2004;113(11):1607.
 60. Torii R, Stettler R, Räber L, et al. Implications of the local haemodynamic forces on the formation and destabilisation of neoatherosclerotic lesions. *EuroPCR 2017 Euro17A-POS1160*. 2017.
 61. Aarts PA, van den Broek SA, Prins GW, Kuiken GD, Sixma JJ, Heethaar RM. Blood platelets are concentrated near the wall and red blood cells, in the center in flowing blood. *Arteriosclerosis (Dallas, Tex)*. 1988;8(6):819-824.

62. Reasor DA, Jr., Mehrabadi M, Ku DN, Aidun CK. Determination of critical parameters in platelet margination. *Annals of biomedical engineering*. 2013;41(2):238-249.
63. Zydney AL, Colton CK. Augmented solute transport in the shear flow of a concentrated suspension. *Physicochemical hydrodynamics*. 1988;10(1):77-96.
64. Schneider S, Nuschele S, Wixforth A, Gorzelanny C, Alexander-Katz A, Netz R, Schneider M. Shear-induced unfolding triggers adhesion of von Willebrand factor fibers. *Proceedings of the National Academy of Sciences*. 2007;104(19):7899-7903.
65. Siediecki C, Lestini BJ, Kottke-Marchant K, Eppell SJ, Wilson DL, Marchant RE. Shear-dependent changes in the three-dimensional structure of human von Willebrand factor. *Blood*. 1996;88(8):2939-2950.
66. Jackson SP, Nesbitt WS, Westein E. Dynamics of platelet thrombus formation. *Journal of Thrombosis and Haemostasis*. 2009;7:17-20.
67. Maxwell MJ, Westein E, Nesbitt WS, Giuliano S, Dopheide SM, Jackson SP. Identification of a 2-stage platelet aggregation process mediating shear-dependent thrombus formation. *Blood*. 2007;109(2):566-576.
68. Colace TV, Diamond SL. Direct observation of von Willebrand factor elongation and fiber formation on collagen during acute whole blood exposure to pathological flow. *Arteriosclerosis, thrombosis, and vascular biology*. 2013;33(1):105-113.
69. Bark DL, Para AN, Ku DN. Correlation of thrombosis growth rate to pathological wall shear rate during platelet accumulation. *Biotechnology and bioengineering*. 2012;109(10):2642-2650.
70. Stettler C, Wandel S, Allemann S, et al. Outcomes associated with drug-eluting and bare-metal stents: a collaborative network meta-analysis. *Lancet (London, England)*. 2007;370(9591):937-948.
71. Claessen BE, Henriques JPS, Jaffer FA, Mehran R, Piek JJ, Dangas GD. Stent Thrombosis: A Clinical Perspective. *JACC: Cardiovascular Interventions*. 2014;7(10):1081-1092.
72. Grouve E, Kristensen S. Stent thrombosis: definitions, mechanisms and prevention. *E-journal of Cardiology Practice*. 2007;32(5).
73. Jiménez J, Davies P. Hemodynamically Driven Stent Strut Design. *Ann Biomed Eng*. 2009;37(8):1483-1494.
74. Seo T, Schachter LG, Barakat AI. Computational study of fluid mechanical disturbance induced by endovascular stents. *Ann Biomed Eng*. 2005;33(4):444-456.
75. Joner M, Nakazawa G, Finn AV, Quee SC, Coleman L, Acampado E, Wilson PS, Skorija K, Cheng Q, Xu X, Gold HK, Kolodgie FD, Virmani R. Endothelial Cell Recovery Between Comparator Polymer-Based Drug-Eluting Stents. *Journal of the American College of Cardiology*. 2008;52(5):333-342.
76. Soucy NV, Feygin JM, Tunstall R, Casey MA, Pennington DE, Huibregtse BA, Barry JJ. Strut tissue coverage and endothelial cell coverage: a comparison between bare metal stent platforms and platinum chromium stents with and without everolimus-eluting coating. *EuroIntervention : journal of EuroPCR in collaboration with the Working Group on Interventional Cardiology of the European Society of Cardiology*. 2010;6(5):630-637.
77. Finn AV, Nakazawa G, Joner M, Kolodgie FD, Mont EK, Gold HK, Virmani R. Vascular Responses to Drug Eluting Stents: Importance of Delayed Healing. *Arteriosclerosis, Thrombosis, and Vascular Biology*. 2007;27(7):1500-1510.
78. Kastrati A, Mehilli J, Dirschinger J, Dotzer F, Schühlen H, Neumann F-J, Fleckenstein M, Pfafferoth C, Seyfarth M, Schömig A. Intracoronary Stenting and Angiographic Results: Strut Thickness Effect on Restenosis Outcome (ISAR-STEREO) Trial. *Circulation*. 2001;103(23):2816-2821.
79. Yoshitomi Y, Kojima S, Yano M, Sugi T, Matsumoto Y, Saotome M, Tanaka K, Endo M, Kuramochi M. Does stent design affect probability of restenosis? A randomized trial comparing Multilink stents with GFX stents. *American Heart Journal*. 2001;142(3):445-451.

80. Pache Jü, Kastrati A, Mehilli J, Schühlen H, Dotzer F, Hausleiter J, Fleckenstein M, Neumann F-J, Sattelberger U, Schmitt C, Müller M, Dirschinger J, Schömig A. Intracoronary stenting and angiographic results: strut thickness effect on restenosis outcome (ISAR-STereo-2) trial. *Journal of the American College of Cardiology*. 2003;41(8):1283-1288.
81. Briguori C, Sarais C, Pagnotta P, Liistro F, Montorfano M, Chieffo A, Sgura F, Corvaja N, Albiero R, Stankovic G, Toutoutzas C, Bonizzoni E, Di Mario C, Colombo A. In-stent restenosis in small coronary arteries: Impact of strut thickness. *Journal of the American College of Cardiology*. 2002;40(3):403-409.
82. Jimenez JM, Prasad V, Yu MD, Kampmeyer CP, Kaakour AH, Wang PJ, Maloney SF, Wright N, Johnston I, Jiang YZ, Davies PF. Macro- and microscale variables regulate stent haemodynamics, fibrin deposition and thrombomodulin expression. *Journal of the Royal Society, Interface*. 2014;11(94):20131079.
83. Otsuka F, Cheng Q, Yahagi K, Acampado E, Sheehy A, Yazdani SK, Sakakura K, Euller K, Perkins LEL, Kolodgie FD, Virmani R, Joner M. Acute Thrombogenicity of a Durable Polymer Everolimus-Eluting Stent Relative to Contemporary Drug-Eluting Stents With Biodegradable Polymer Coatings Assessed Ex Vivo in a Swine Shunt Model. *JACC: Cardiovascular Interventions*. 2015;8(9):1248-1260.
84. Puricel S, Cuculi F, Weissner M, Schmermund A, Jamshidi P, Nyffenegger T, Binder H, Eggebrecht H, Münzel T, Cook S. Bioresorbable coronary scaffold thrombosis: multicenter comprehensive analysis of clinical presentation, mechanisms, and predictors. *Journal of the American College of Cardiology*. 2016;67(8):921-931.
85. Cassese S, Byrne RA, Ndrepepa G, Kufner S, Wiebe J, Repp J, Schunkert H, Fusaro M, Kimura T, Kastrati A. Everolimus-eluting bioresorbable vascular scaffolds versus everolimus-eluting metallic stents: a meta-analysis of randomised controlled trials. *The Lancet*. 387(10018):537-544.
86. Ellis SG, Kereiakes DJ, Metzger DC, Caputo RP, Rizik DG, Teirstein PS, Litt MR, Kini A, Kabour A, Marx SO. Everolimus-eluting bioresorbable scaffolds for coronary artery disease. *New England Journal of Medicine*. 2015;373(20):1905-1915.
87. Bourantas CV, Onuma Y, Farooq V, Zhang Y, Garcia-Garcia HM, Serruys PW. Bioresorbable scaffolds: Current knowledge, potentialities and limitations experienced during their first clinical applications. *International Journal of Cardiology*. 2013;167(1):11-21.
88. Serruys PW, Onuma Y, García-García HM, et al. Dynamics of vessel wall changes following the implantation of the Absorb everolimus-eluting bioresorbable vascular scaffold: a multi-imaging modality study at 6, 12, 24 and 36 months. *EuroIntervention : journal of EuroPCR in collaboration with the Working Group on Interventional Cardiology of the European Society of Cardiology*. 2014;9(11):1271-1284.
89. Ormiston JA, Serruys PW, Onuma Y, et al. First serial assessment at 6 months and 2 years of the second generation of absorb everolimus-eluting bioresorbable vascular scaffold: a multi-imaging modality study. *Circ Cardiovasc Interv*. 2012;5(5):620-632.
90. Otsuka F, Pacheco E, Perkins LEL, Lane JP, Wang Q, Kamberi M, Frie M, Wang J, Sakakura K, Yahagi K, Ladich E, Rapoza RJ, Kolodgie FD, Virmani R. Long-Term Safety of an Everolimus-Eluting Bioresorbable Vascular Scaffold and the Cobalt-Chromium XIENCE V Stent in a Porcine Coronary Artery Model. *Circulation: Cardiovascular Interventions*. 2014;7(3):330-342.
91. Stone GW, Gao R, Kimura T, Kereiakes DJ, Ellis SG, Onuma Y, Cheong W-F, Jones-McMeans J, Su X, Zhang Z, Serruys PW. 1-year outcomes with the Absorb bioresorbable scaffold in patients with coronary artery disease: a patient-level, pooled meta-analysis. *The Lancet*. 387(10025):1277-1289.
92. Sotomi Y, Tateishi H, Suwannasom P, et al. Quantitative assessment of the stent/scaffold strut embedment analysis by optical coherence tomography. *The International Journal of Cardiovascular Imaging*. 2016;32:871-883.

93. Nakazawa G, Yazdani SK, Finn AV, Vorpahl M, Kolodgie FD, Virmani R. Pathological Findings at Bifurcation Lesions: The Impact of Flow Distribution on Atherosclerosis and Arterial Healing After Stent Implantation. *Journal of the American College of Cardiology*. 2010;55(16):1679-1687.
94. Finn AV. Differential response of delayed healing and persistent inflammation at sites of overlapping sirolimus-or paclitaxel-eluting stents. *Circulation*. 2005;112(2):270.
95. Simon C, Palmaz JC, Sprague EA. Influence of topography on endothelialization of stents: clues for new designs. *Journal of long-term effects of medical implants*. 2000;10(1-2):143-151.
96. Finn AV, Joner M, Nakazawa G, Kolodgie F, Newell J, John MC, Gold HK, Virmani R. Pathological Correlates of Late Drug-Eluting Stent Thrombosis: Strut Coverage as a Marker of Endothelialization. *Circulation*. 2007;115(18):2435-2441.
97. Farooq V, Serruys PW, Heo JH, et al. Intracoronary optical coherence tomography and histology of overlapping everolimus-eluting bioresorbable vascular scaffolds in a porcine coronary artery model: the potential implications for clinical practice. *JACC Cardiovascular interventions*. 2013;6(5):523-532.
98. Kaneda H, Ma J, Morita T. Stent Underexpansion in Early Drug-Eluting Stent Thrombosis. *JACC: Cardiovascular Interventions*. 2009;2(8):807-807.
99. Foin N, Torii R, Mattesini A, Wong P, Di Mario C. Biodegradable vascular scaffold: is optimal expansion the key to minimising flow disturbances and risk of adverse events? *EuroIntervention : journal of EuroPCR in collaboration with the Working Group on Interventional Cardiology of the European Society of Cardiology*. 2015;10(10):1139-1142.
100. Unzué Vallejo L, Hernández Hernández F, Velázquez Martín MT, García Tejada J, Albarrán González-Trevilla A, Tascón Pérez J. Role of Intravascular Ultrasound in Stent Thrombosis. *Revista Española de Cardiología (English Edition)*. 2013;66(04):317-319.
101. Fujii K, Carlier SG, Mintz GS, Yang Y-m, Moussa I, Weisz G, Dangas G, Mehran R, Lansky AJ, Kreps EM, Collins M, Stone GW, Moses JW, Leon MB. Stent underexpansion and residual reference segment stenosis are related to stent thrombosis after sirolimus-eluting stent implantation: An intravascular ultrasound study. *Journal of the American College of Cardiology*. 2005;45(7):995-998.
102. Alfonso F, Suárez A, Angiolillo DJ, Sabaté M, Escaned J, Moreno R, Hernández R, Bañuelos C, Macaya C. Findings of intravascular ultrasound during acute stent thrombosis. *Heart*. 2004;90(12):1455-1459.
103. Zhang YJ, Bourantas CV, Muramatsu T, Iqbal J, Farooq V, Diletti R, Campos CA, Onuma Y, Garcia-Garcia HM, Serruys PW. Comparison of acute gain and late lumen loss after PCI with bioresorbable vascular scaffolds versus everolimus-eluting stents: an exploratory observational study prior to a randomised trial. *EuroIntervention : journal of EuroPCR in collaboration with the Working Group on Interventional Cardiology of the European Society of Cardiology*. 2014;10(6):672-680.
104. Suwannasom P, Sotomi Y, Ishibashi Y, et al. The Impact of Post-Procedural Asymmetry, Expansion, and Eccentricity of Bioresorbable Everolimus-Eluting Scaffold and Metallic Everolimus-Eluting Stent on Clinical Outcomes in the ABSORB II Trial. *JACC: Cardiovascular Interventions*. 2016;9(12):1231-1242.
105. Foin N, Lee R, Bourantas C, et al. Bioresorbable vascular scaffold radial expansion and conformation compared to a metallic platform: insights from in vitro expansion in a coronary artery lesion model. *EuroIntervention : journal of EuroPCR in collaboration with the Working Group on Interventional Cardiology of the European Society of Cardiology*. 2016;12(7):834-844.
106. Javadzadegan A, Yong AS, Chang M, Ng AC, Yiannikas J, Ng MK, Behnia M, Kritharides L. Flow recirculation zone length and shear rate are differentially affected by stenosis severity in human coronary arteries. *Am J Physiol Heart Circ Physiol*. 2013;304(4):H559-566.
107. Guagliumi G, Sirbu V, Musumeci G, Gerber R, Biondi-Zoccai G, Ikejima H, Ladich E, Lortkipanidze N, Matiashvili A, Valsecchi O, Virmani R, Stone GW. Examination of the in vivo mechanisms of late drug-

- eluting stent thrombosis: findings from optical coherence tomography and intravascular ultrasound imaging. *JACC Cardiovasc Interv.* 2012;5(1):12-20.
108. Holme PA, Orvim U, Hamers MJ, Solum NO, Brosstad FR, Barstad RM, Sakariassen KS. Shear-induced platelet activation and platelet microparticle formation at blood flow conditions as in arteries with a severe stenosis. *Arterioscler Thromb Vasc Biol.* 1997;17:646–653.
 109. Capodanno D, Gori T, Nef H, et al. Percutaneous coronary intervention with everolimus-eluting bioresorbable vascular scaffolds in routine clinical practice: early and midterm outcomes from the European multicentre GHOST-EU registry. *EuroIntervention : journal of EuroPCR in collaboration with the Working Group on Interventional Cardiology of the European Society of Cardiology.* 2014.
 110. Ishibashi Y, Onuma Y, Muramatsu T, Nakatani S, Iqbal J, García-García HM, Bartorelli AL, Whitbourn RJ, Abizaid A, Serruys PW. Lessons learned from acute and late scaffold failures in the ABSORB EXTEND trial. *EuroIntervention : journal of EuroPCR in collaboration with the Working Group on Interventional Cardiology of the European Society of Cardiology.* 2014;10(4):449-457.
 111. Ormiston JA, De Vroey F, Serruys PW, Webster MWI. Bioresorbable Polymeric Vascular Scaffolds: A Cautionary Tale. *Circulation: Cardiovascular Interventions.* 2011;4(5):535-538.
 112. Di Mario C, Caiazzo G. Biodegradable stents: the golden future of angioplasty? *The Lancet.* 2014.
 113. Gomez-Lara J, Radu M, Brugaletta S, et al. Serial Analysis of the Malapposed and Uncovered Struts of the New Generation of Everolimus-Eluting Bioresorbable Scaffold With Optical Coherence Tomography. *JACC: Cardiovascular Interventions.* 2011;4(9):992-1001.
 114. Joner M, Finn AV, Farb A, Mont EK, Kolodgie FD, Ladich E, Kutys R, Skorija K, Gold HK, Virmani R. Pathology of Drug-Eluting Stents in Humans: Delayed Healing and Late Thrombotic Risk. *Journal of the American College of Cardiology.* 2006;48(1):193-202.
 115. Nakano M, Yahagi K, Otsuka F, Sakakura K, Finn AV, Kutys R, Ladich E, Fowler DR, Joner M, Virmani R. Causes of Early Stent Thrombosis in Patients Presenting With Acute Coronary Syndrome: An Ex Vivo Human Autopsy Study. *Journal of the American College of Cardiology.* 2014;63(23):2510-2520.

Table 1. Patient Studies on Atherosclerosis and Restenosis

<i>Reference</i>	<i>No. of Subjects</i>	<i>Follow-Up (mo)</i>	<i>Imaging Modality</i>	<i>Results</i>
Atherosclerosis				
Stone et al. (2003) ¹⁵	8	6	Angiography, IVUS	Regions of low ESS showed progressive atherosclerosis and outward remodelling.
Stone et al. (2006) ⁴⁶	13	8±2	Angiography, IVUS	Compared to moderate/high ESS, low ESS showed plaque progression (p=0.009).
Samady et al. (2011) ⁴⁷	20	6	Angiography, IVUS	Regions of low ESS developed progression of plaque area (p=0.027), necrotic core (p<0.001) and decrease in vessel (p<0.001) and lumen area (p<0.001) as compared to regions of intermediate ESS. Compared to intermediate ESS, high ESS developed progression of necrotic core (p<0.001), dense calcium (p<0.001) regression of fibrous (p<0.001) and fibrofatty (p<0.001) tissue and increase in vessel (p<0.001) and lumen area (p<0.001).
Stone et al. (2012) ¹⁷	506	8±2	Angiography, IVUS	Low ESS is associated with plaque enlargement and lumen narrowing, the main message being ESS is a predictor of clinical outcomes.
Vergallo et al. (2014) ⁴⁸	21	-	Angiography, OCT	Regions exposed to low ESS is linked to larger lipid burden (p=0.019), thinner fibrous cap (p=0.004) and higher prevalence of thin-cap fibroatheroma (p=0.037).
Hung et al. (2016) ⁴⁹	24	24	Angiography, IVUS	Low ESS was linked to plaque progression (p<0.0001) and constrictive remodelling (p=0.04).
Restenosis				
Wentzel et al. (2001) ⁵⁰	14	6	Angiography, IVUS	Neointimal thickness at follow up is inversely related to shear stress in BMS. Thickness = 0.59– 0.08*Shear Stress, p < 0.05.
Gijssen et al. (2003) ⁵¹	6	6	Angiography, IVUS	There was a negative linear relation between neointimal thickness and shear stress. Thickness = 0.21 – 0.24*Shear Stress, R ² =0.24, p < 0.001.
Papafaklis et al. (2008) ⁵²	14	6	Angiography, IVUS	In stent restenosis is inversely related to ESS after coronary with the equation: Thickness = 0.28– 0.057*Shear Stress, p<0.001. Vascular brachytherapy diminishes the inverse relationship between restenosis and ESS.
Papafaklis et al. (2010) ⁵³	30	6	IVUS	Low ESS is inversely related to neointimal thickness for both BMS (slope = -0.05mm/Pa, p = 0.001) and DES (slope = - 0.05mm/Pa, p = 0.016).
Bourantas et al. (2014) ⁵⁴	6	6 or 12	Angiography, OCT, IVUS	In scaffolded segments models the ESS estimated by the fusion of IVUS and X-ray angiography differs from the ESS derived from the fusion of OCT and X-ray imaging. The correlation coefficient between ESS and neointima thickness is increased in OCT based modelling comparing to IVUS based reconstructions.
Bourantas et al. (2014) ⁵⁵	12	12	OCT	Low ESS was associated with increased neointima thickness at 1 year follow up in BRS (correlation coefficient range: -0.140 to -0.662).
Bourantas et al. (2015) ⁵⁶	43	13	Angiography, IVUS	ESS determines neointimal formation in both BMS (p < 0.001) and BES (p=0.002) and is a predictor of an increased necrotic core component in BMS.
Shishido et al. (2016) ⁵⁷	374	6-10	Angiography, IVUS	Low ESS after BMS implantation is associated with in stent hyperplasia. Post PCI ESS is not associated with in stent restenosis requiring repeat PCI.

A summary on patient studies that look the effect of shear stress on atherosclerosis and restenosis. Most atherosclerosis showed an inverse association between ESS and plaque or neointima burden. BES indicates biolimus eluting stents; BMS, bare metal stents; BRS, bioresorbable scaffolds; ESS, endothelial shear stress; IVUS, intravascular ultrasound; OCT, optical coherence tomography; and PCI, percutaneous coronary intervention.

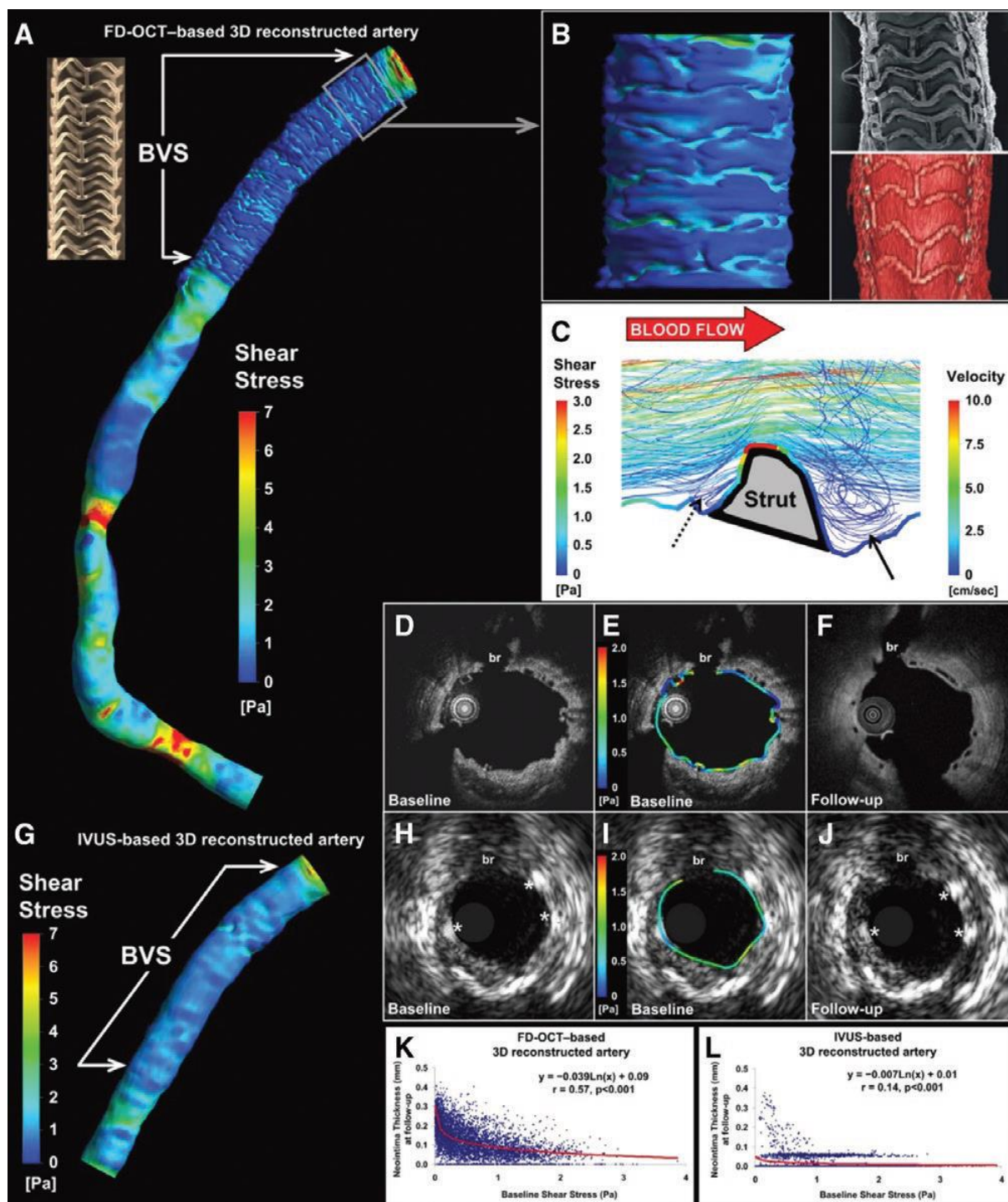


Figure 1. Optical coherence tomography (OCT)-based reconstruction and blood flow simulation immediately after scaffold implantation. This is an example of the use of high-resolution imaging modalities for the prediction of local hemodynamics and endothelial shear stress (ESS) after Absorb bioresorbable vascular scaffold (BVS) implantation. A magnified view of the OCT-derived lumen surface (A), revealing the strut architecture in the OCT-derived lumen surface (B). Protruding struts affect the local ESS distribution with higher values noted on top of the struts and lower values in the interstrut areas (B). Flow streamlines in a longitudinal cross-section (C); flow disturbance and recirculation regions around the struts regions (arrow and dotted arrow). Corresponding OCT cross-sectional images (evident by the side branch [br]) at baseline (D), ESS distribution (E), and 2-y follow-up (F). Intravascular ultrasound (IVUS)-based reconstruction of the scaffolded segment at baseline (G) with the ESS shown in a color-coded map (G). IVUS cross-sectional images at baseline (H) and 2-y followup (J) corresponding to the OCT images. The lower IVUS resolution allows a rough assessment of BVS struts (*) and cannot detect the neointima tissue. Note the smoother ESS distribution compared with the OCT-based model. A stronger correlation was noted between the baseline ESS and neointima thickness at 2 y in the OCT-based model (K, $R^2=0.50$) compared with the IVUS-based reconstruction (L, $R^2=0.13$). Reprinted from Papafaklis et al³ with permission. Copyright ©2013, Europa Digital & Publishing. 3D indicates 3-dimensional.

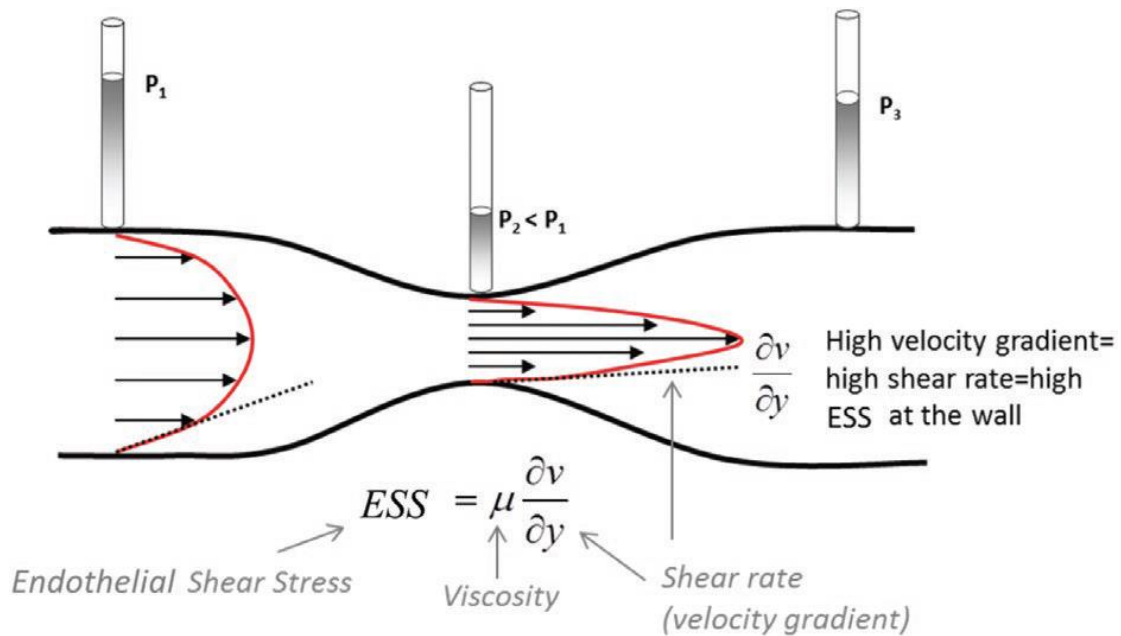


Figure 2. Shear rate and endothelial shear stress (ESS) definition. Shear rate is the velocity gradient along the diameter of the vessel. ESS is derived from the velocity gradient near the wall (shear rate) multiplied by the viscosity of the blood (μ). It has the dimension of force per unit area and is expressed generally in Pascal or dyne/cm² (1 Pa=10 dyne/cm²). In a straight cylindrical vessel of a radius r with a developed parabolic laminar flow profile (Poiseuille flow), ESS can be evaluated from the Hagen–Poiseuille equation: $ESS=4Q \cdot \mu / (\pi r^3)$, where Q is the flow-rate, μ the fluid viscosity, r the tube radius. Adapted from Foin et al⁵ with permission. Copyright ©2017.

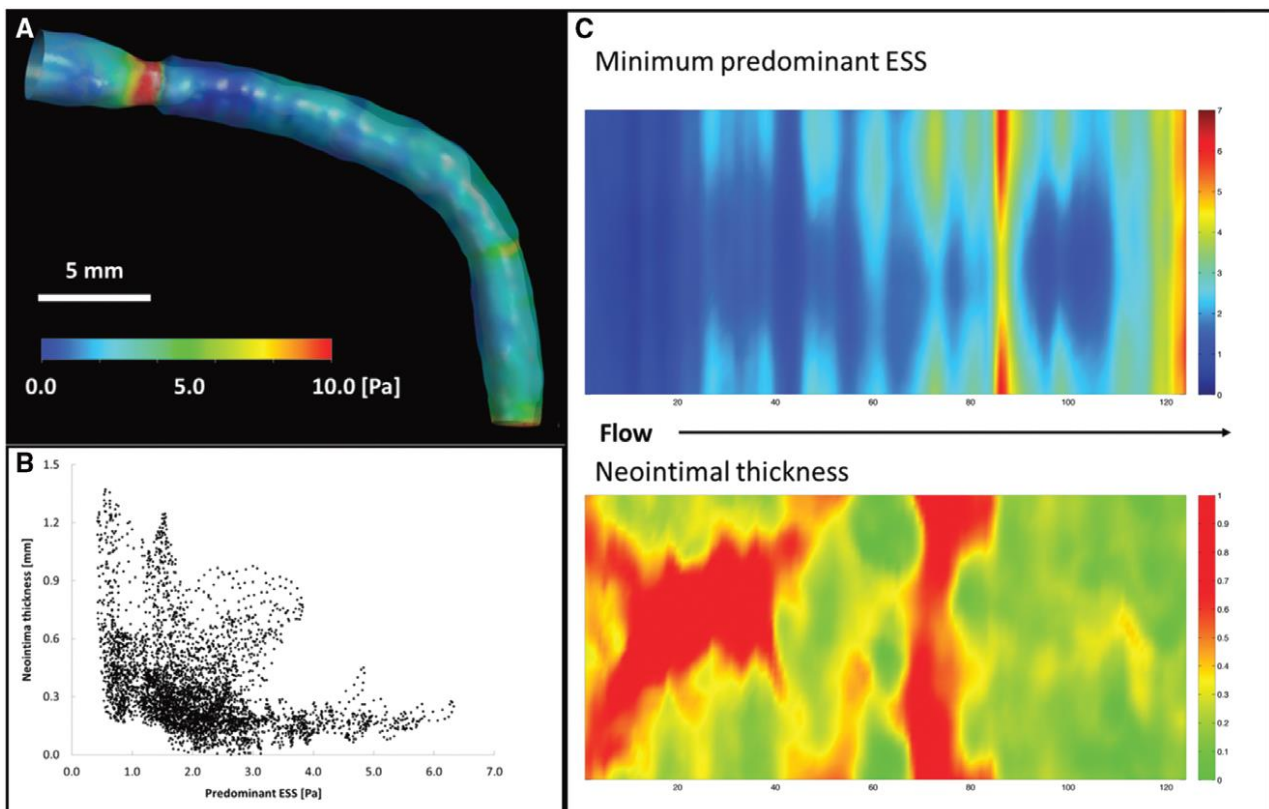


Figure 3. Correlation between baseline endothelial shear stress (ESS) and thickness of neointima in a patient with 3.7 y of follow-up after stent implantation. **A**, ESS map on the baseline 3-dimensional vascular model (transparent) and vessel anatomy at the follow-up (gray surface inside). **B**, Point-to-point association between the baseline ESS and neointimal thickness within the stented segment, showing inverse-proportional correlation. **C**, Spread-out plots of ESS (**top**) and neointimal thickness (**bottom**) in the stented segment, demonstrating spatial relationship between low ESS and neointimal thickening.

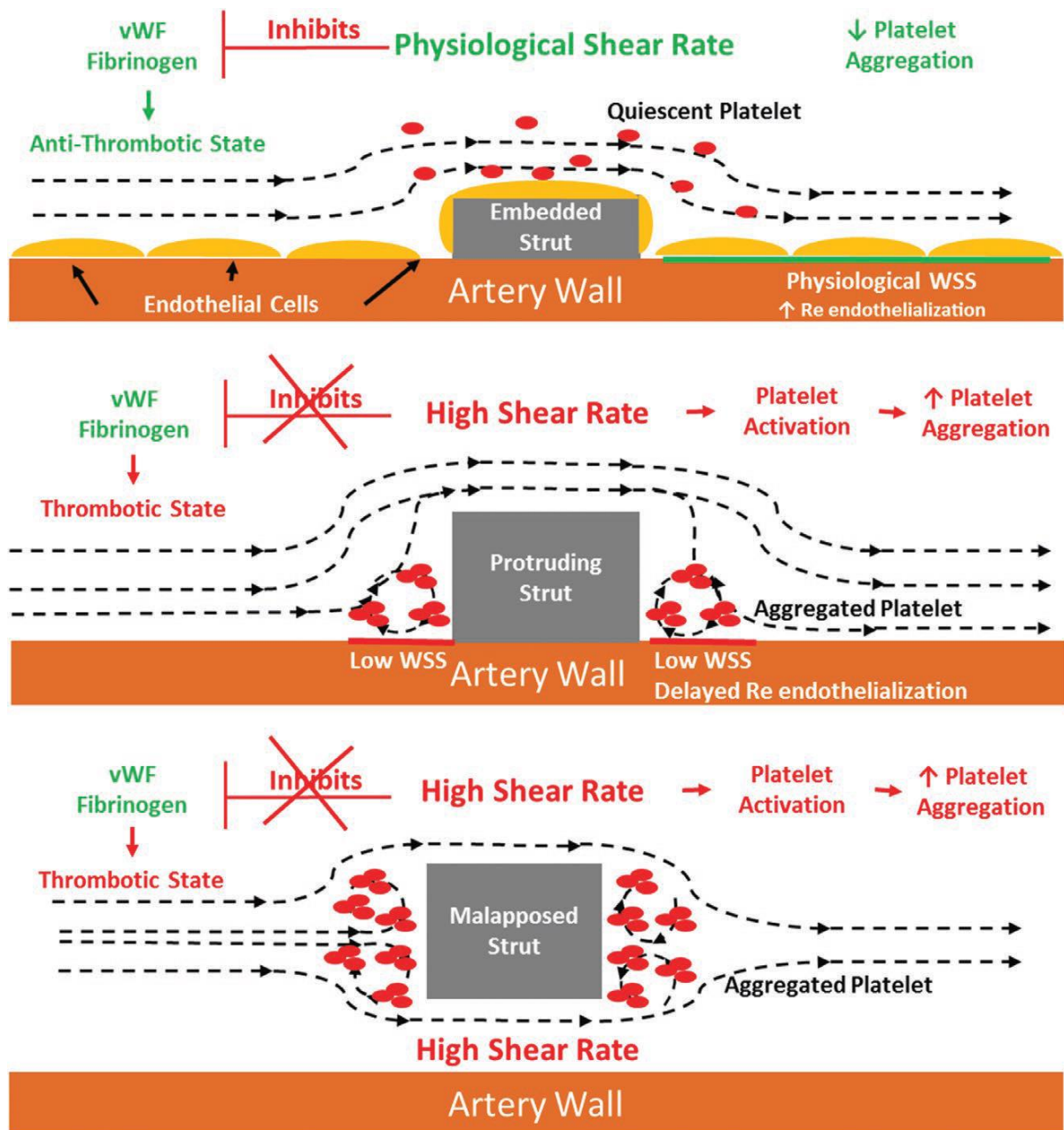


Figure 4. Stent strut protrusion and thrombosis. Embedded struts disrupt blood flow the least out of the 3 scenarios and has the lowest area of recirculation and physiological levels of shear rate. Hence, activator proteins like vWF (Von Willebrand factor) are not activated, and platelet adhesion and aggregation remain at a minimum. Malapposed struts have regions of high shear rate both at the top and bottom of the strut and a larger surface area for adhesion proteins to bind to, creating a thrombogenic surface as compared with a protruding strut. At high shear rates, platelets are activated via the vWF binding to glycoprotein (GP) Ib and GP IIb/IIIa receptors^{13,108} resulting in clot formation and potentially thrombosis formation.^{6,7} Top panels adapted from Koskinas et al¹³ with permission. Copyright ©2012, Elsevier.

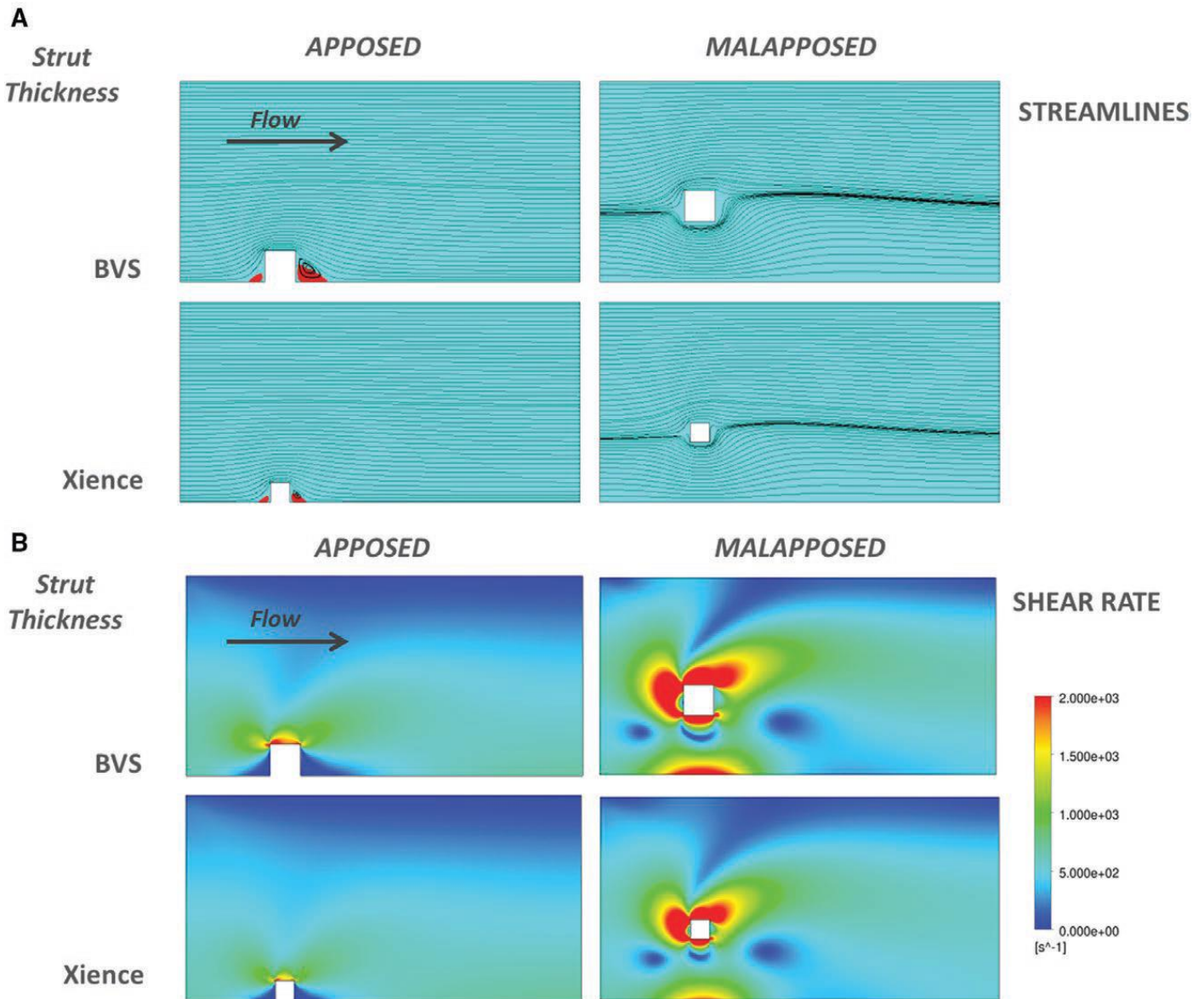


Figure 5. Impact of strut thickness on blood flow profiles for model simulating case of well-apposed and malapposed drug-eluting stents (DES) and bioresorbable scaffolds (BRS) struts. **A**, Simulated blood flow streamlines (**top**) for the different cases of strut apposition: (1) apposed and (2) malapposed (with strut to wall distance=300 μm). Models are representative of a 3-mm diameter straight coronary artery flow with a parabolic upstream velocity profile and a peak velocity of 50 cm/s. The 2 strut thicknesses are considered to correspond to a total strut thickness (strut+coating) of 156 μm (Absorb BVS) and 97 μm (Xience DES). **B**, Corresponding shear rate profile in blood around stent strut simulated for each case (**bottom**) shows that flow disturbances and high shear rates (red) are increased primarily in thicker and malapposed struts. Reprinted from Foin et al99 with permission. Copyright ©2015, Europa Digital & Publishing.